

Boundary knot method based on geodesic distance for anisotropic problems

Bangti Jin, Wen Chen *

Department of Engineering Mechanics, Hohai University, No. 1 Xikang Road, Nanjing City, Jiangsu Province 210098, China

Received 18 June 2005; received in revised form 9 September 2005; accepted 7 November 2005

Available online 17 February 2006

Abstract

The radial basis function (RBF) collocation techniques for the numerical solution of partial differential equation problems are increasingly popular in recent years thanks to their striking merits being inherently meshless, integration-free, and highly accurate. However, the RBF-based methods have markedly been limited to handle isotropic problems due to the use of the isotropic Euclidean distance. This paper makes the first attempt to use the geodesic distance with the RBF-based boundary knot method (BKM) to solve 2D and 3D anisotropic Helmholtz-type and convection-diffusion problems. This approach is mathematically simple and easy to implement, and spectral convergence is numerically observed for problems under complex-shaped boundary. Numerical results show that the BKM based on the geodesic distance can produce highly accurate solutions of anisotropic problems with a relatively small number of knots. This study provides a promising strategy for the RBF-based methods to effectively solve anisotropic problems.

© 2005 Elsevier Inc. All rights reserved.

Keywords: Radial basis function; Geodesic distance; Boundary knot method; Anisotropic materials; Meshless method

1. Introduction

The function expressed in the Euclidean distance variable is usually termed a radial basis function (RBF) in literature. This is because they are radially isotropic due to the rotational invariance, and have become de facto the standard distance function of the most practical use today. For instance, in multivariate scattered data processing, the RBF approach has now become the method of choice [13]. Since Kansa's pioneering work [18], the RBF has also increasingly been used to solve various partial differential equation (PDE) problems numerically [12,17,29,30]. However, the RBF-based approaches have long been limited to isotropic PDE problems due to the fact that the conventional RBFs are based on the isotropic Euclidean distance variable.

Anisotropic materials are ubiquitous in nature. Among known examples are crystals, wood, sedimentary rocks, laminated sheets, fiber-reinforced composites, and thin films etc. Their various physical behaviors are usually described by corresponding anisotropic partial differential equations, and the accurate numerical

* Corresponding author.

E-mail address: wenc66@yahoo.com (W. Chen).

solution of these equations is imperative in a broad range of scientific and engineering applications. In this regard, the traditional numerical methodology [24] is to transform an anisotropic problem into an isotropic one, and as a byproduct of this transformation, the boundary conditions often become much more complicated. Then the standard numerical solution techniques, e.g., FEM, FDM as well as the Euclidean distance based RBF methods, are used to solve the transformed isotropic problems. An alternative strategy is to embed the anisotropy in the numerical algorithm [26] and then solve the problem directly without using the transformation. In this study, we will use the latter strategy in the RBF-based boundary knot method (BKM) [11] to solve anisotropic partial differential equation problems.

Our new approach is to replace the Euclidean distance with the anisotropic geodesic distance in the radial basis function of the BKM [9]. This novel scheme is tested to the anisotropic Helmholtz-type and convection-diffusion problems under complicated geometry, and its convergence is numerically investigated. To our best knowledge, this paper makes the first attempt to use the geodesic distance with the RBF-based method to solve the anisotropic partial differential equation problems. In Section 2, we give a brief introduction of the BKM and then geodesic distance, followed in Section 3 by numerical results and discussions. Finally, Section 4 concludes this paper with some remarks based on numerical experiments results and analyses.

2. Anisotropic distance, RBF and boundary knot method

Let Ω be an open bounded domain in \mathbf{R}^d , where d is the dimensionality of the space, and $\Gamma = \partial\Omega$ represents its boundary. Without loss of generality, we consider the Helmholtz equation under anisotropic media

$$\sum_{i=1}^d \sum_{j=1}^d k_{ij} \frac{\partial^2 u(x)}{\partial x_i \partial x_j} + \lambda^2 u = f(x), \quad x = (x_1, x_2, \dots, x_d) \in \Omega, \tag{1}$$

where $\mathbf{K}=\{k_{ij}\}$ is the constant material tensor assumed to be positive-definite. For example, \mathbf{K} is given in 3D cases by

$$K = \begin{Bmatrix} k_{11} & k_{12} & k_{13} \\ k_{21} & k_{22} & k_{23} \\ k_{31} & k_{32} & k_{33} \end{Bmatrix}.$$

It is well-known that the smaller the determinant of k_{ij} , the more asymmetric and anisotropic are the field and flux vectors, and consequently, the more difficult it is to get the accurate numerical solution. The constant λ is a real number. In case that the λ is purely imaginary, the equation is also known as the modified Helmholtz equation, and it can be rewritten as

$$\sum_{i=1}^d \sum_{j=1}^d k_{ij} \frac{\partial^2 u(x)}{\partial x_i \partial x_j} - \lambda^2 u = f(x), \quad x = (x_1, x_2, \dots, x_d) \in \Omega \tag{2}$$

so as to eliminate the imaginary unit. In this study, we also consider anisotropic convection-diffusion equation

$$\sum_{i=1}^d \sum_{j=1}^d k_{ij} \frac{\partial^2 u(x)}{\partial x_i \partial x_j} + \mathbf{v} \cdot \nabla u - \eta^2 u = f(x), \quad x = (x_1, x_2, \dots, x_d) \in \Omega, \tag{3}$$

where \mathbf{v} is a velocity vector. The governing Eqs. (1)–(3) are typically subjected to the following boundary conditions:

$$\begin{cases} u(x) = g(x), & x \in \Gamma_1, \\ q(x) = h(x), & x \in \Gamma_2, \end{cases} \tag{4}$$

where Γ_1 and Γ_2 are the two disjointed parts constituting the boundary Γ . The flux $q(x)$ through the boundary Γ_1 is given by

$$q(x) = \frac{\partial u}{\partial v^+}, \tag{5}$$

where v is the normal vector to the boundary Γ , and

$$\frac{\partial u}{\partial v^+} = \sum_{i=1}^d \sum_{j=1}^d k_{ij} \cos(v, x_i) \frac{\partial u}{\partial x_j}, \quad (6)$$

where $\cos(v, x_i)$ are the directional cosine of the outward normal vector v to the boundary Γ .

In the RBF-based BKM framework, the anisotropic problems are solved in a two-step approach. Firstly, we evaluate an approximate particular solution by means of the dual reciprocity method (DRM) and RBFs [22], and secondly, its homogeneous solution is approximated via the nonsingular general solution formulation. Namely, the solution $u(x)$ is split by

$$u(x) = u_h(x) + u_p(x), \quad (7)$$

where $u_h(x)$ and $u_p(x)$ are the homogeneous and particular solutions, respectively. The latter satisfies the governing equation but not necessarily the boundary conditions. To evaluate the particular solution, we approximate the source term $f(x)$ by

$$f(x) = \sum_{k=1}^L c_k \phi(R_k), \quad (8)$$

where c_k are unknown coefficients, ϕ denotes a radial basis function, and L is the number of knots. In this study, the standard Euclidean distance $r_k = \|x - x_k\|_2$ is replaced by the geodesic distance R_k defined between $x = (x_1, x_2, \dots, x_d)$ and $x_k = (x_{k1}, x_{k2}, \dots, x_{kd})$ as below [9]:

$$R_k^2 = \sum_{i=1}^d \sum_{j=1}^d k^{ij} (x_i - x_{ki})(x_j - x_{kj}) = (x - x_k)^T \mathbf{K}^{-1} (x - x_k). \quad (9)$$

$\mathbf{K}^{-1} = \{k^{ij}\}$ is the inverse of the anisotropic coefficient matrix K . In case of isotropic media, K is an identity matrix and the geodesic distance is reduced to the Euclidean distance. It is noted that the RBF ϕ used in the DRM can either be isotropic based on the Euclidean distance or an anisotropic geodesic distance. In case of the conditionally positive definite RBF ϕ , a polynomial term need be included in the above summation (8) to guarantee the non-singularity of the RBF interpolation matrix. By collocating Eq. (8) at all the nodes, we can uniquely determine

$$\mathbf{c} = \mathbf{A}_\phi^{-1} \mathbf{f}, \quad (10)$$

where \mathbf{A}_ϕ is an interpolation matrix, $\mathbf{c} = (c_1, c_2, \dots, c_L)^T$ is the unknown coefficient vector. Once \mathbf{c} is determined, the particular solution $u_p(x)$ can be obtained by using the DRM

$$u_p(x) = \sum_{k=1}^L c_k \psi(R_k), \quad (11)$$

where the RBF ψ is related to the governing differential operator. For a detailed account of the use of RBFs in the DRM and the derivation of ψ for a given ϕ , we refer to Refs. [4,15]. Another simple approach is that we first choose ψ and accordingly determine ϕ through a simple differentiation process [11].

In the second step, the homogeneous solution $u_h(x)$ is obtained by using boundary type techniques such as the method of fundamental solutions (MFS) [14] and boundary knot method [11]. The basic idea of the BKM is to approximate the solution of a partial differential equation by a linear combination of nonsingular general solutions instead of singular fundamental solutions in the MFS. Thus it avoids the controversial requirement in the MFS of constructing a fictitious boundary outside the physical domain. The BKM has been well-established for the isotropic problems [5–7,10,11]. But like other RBF-based numerical techniques, the BKM has never successfully been applied to anisotropic problems.

The nonsingular general solution $u^\#(x)$ of the anisotropic Helmholtz equation in \mathbf{R}^d is given by

$$u^\#(x) = \frac{1}{2\pi} \left(\frac{\lambda}{2\pi R} \right)^{d/2-1} J_{d/2-1}(\lambda R), \quad d \geq 2, \quad (12)$$

where J_m is the Bessel function of the first kind of order m , and R is the geodesic distance between the source and response points. Similarly, the nonsingular general solution of the anisotropic modified Helmholtz equation in \mathbf{R}^d is given by

$$u^\#(x) = \frac{1}{2\pi} \left(\frac{\lambda}{2\pi R} \right)^{d/2-1} I_{d/2-1}(\lambda R), \quad d \geq 2, \tag{13}$$

where I_m is the modified Bessel function of the first kind of order m . Analogously, the nonsingular general solution of the anisotropic convection-diffusion equation is given by

$$u^\#(x) = \frac{1}{2\pi} \left(\frac{\lambda}{2\pi R} \right)^{d/2-1} e^{-\frac{\mathbf{v} \cdot \mathbf{K}^{-1} \mathbf{r}}{2}} I_{d/2-1}(\eta R), \quad d \geq 2, \tag{14}$$

where \mathbf{r} is the distance vector between the response and source points, and η is defined as

$$\eta = \left(\lambda^2 + \frac{\mathbf{v} \cdot \mathbf{K}^{-1} \mathbf{v}}{4} \right)^{1/2}. \tag{15}$$

The general solutions $u^\#(x)$ of the 2D and 3D Helmholtz operator are given by

$$u^\#(x) = \begin{cases} J_0(\lambda R), & x \in \mathbf{R}^2, \\ \frac{\sin \lambda R}{R}, & x \in \mathbf{R}^3. \end{cases} \tag{16}$$

For the modified Helmholtz operator we have

$$u^\#(x) = \begin{cases} I_0(\lambda R), & x \in \mathbf{R}^2, \\ \frac{\sinh \lambda R}{R}, & x \in \mathbf{R}^3, \end{cases} \tag{17}$$

where \sinh is the hyperbolic sine function. And for the convection-diffusion operator we have

$$u^\#(x) = \begin{cases} I_0(\eta R) e^{-\frac{\mathbf{v} \cdot \mathbf{K}^{-1} \mathbf{r}}{2}}, & x \in \mathbf{R}^2, \\ \frac{\sinh \eta R}{R} e^{-\frac{\mathbf{v} \cdot \mathbf{K}^{-1} \mathbf{r}}{2}}, & x \in \mathbf{R}^3. \end{cases} \tag{18}$$

In the BKM, the solution $u_h(x)$ of the homogeneous problem is approximated by

$$u_h(x) = \sum_{j=1}^N a_j u^\#(x - x_j), \quad x \in \Omega, \tag{19}$$

where x_j are collocation points on the boundary, and a_j unknown coefficients.

The approximate solution $u_h(x)$ satisfies the governing partial differential equation but does not necessarily satisfy the boundary conditions, which can be enforced by collocating boundary conditions at $\{x_i\}$. Finally we get the BKM discretization system of linear equations

$$\begin{cases} \sum_{j=1}^N a_j u^\#(x_i - x_j) = g(x_i) - u_p(x_i), & x_i \in \Gamma_1, \\ \sum_{j=1}^N a_j \frac{\partial u^\#(x_i - x_j)}{\partial v^+} = h(x_i) - \frac{\partial u_p(x_i)}{\partial v^+}, & x_i \in \Gamma_2. \end{cases} \tag{20}$$

In a short form, Eq. (20) is rewritten in a matrix equation form

$$\mathbf{A} \mathbf{a} = \mathbf{b}, \tag{21}$$

where $\mathbf{a} = (a_1, a_2, \dots, a_N)^T$, \mathbf{b} is a known data vector, and $\mathbf{A} = \{A_{ij}\}$ is the interpolation matrix with entries A_{ij} defined by

$$A_{ij} = \begin{cases} u^\#(x_i - x_j), & x_i \in \Gamma_1, \\ \frac{\partial u^\#(x_i - x_j)}{\partial v^+}, & x_i \in \Gamma_2. \end{cases} \tag{22}$$

By solving the matrix Eq. (21), we get the values of the expansion coefficients a_j . Then it is straightforward to evaluate the numerical solution $u(x)$ at any interior points by

$$u(x) = u_p(x) + u_h(x) = \sum_{k=1}^L c_k \psi(R_k) + \sum_{j=1}^N a_j u^\#(x - x_j). \tag{23}$$

3. Numerical results and discussion

In this section the convergence of the present anisotropic BKM scheme is numerically examined, and its application to anisotropic problems under complicated geometry is illustrated. Since the DRM in conjunction with the RBFs is well-established in the literature [19,22] for inhomogeneous problems, we consider only homogeneous problems in the present study.

To investigate the convergence of the BKM, we first calculate homogeneous Helmholtz-type and convection-diffusion problems with the two simple geometries: a circular domain $\Omega = \{(x_1, x_2) | x_1^2 + x_2^2 < 1\}$ and a square domain $\Omega = \{(x_1, x_2) | -1 < x_1, x_2 < 1\}$. To measure the accuracy of the approximation, the average relative error $rerr(u)$, average absolute error $aerr(u)$ and maximum error $merr(u)$ defined as below are employed

$$rerr(u) = \frac{\sqrt{\sum_{j=1}^L (u_j - \tilde{u}_j)^2}}{\sum_{j=1}^L (u_j)^2}, \tag{24a}$$

$$aerr(u) = \sqrt{\frac{1}{L} \sum_{j=1}^L (u_j - \tilde{u}_j)^2}, \tag{24b}$$

$$merr(u) = \max_j |u_j - \tilde{u}_j|, \tag{24c}$$

where u_j and \tilde{u}_j are respectively the analytical and numerical solutions at the node $x_j \in \Omega$, and L is the total number of internal nodes of interest, 10,000 nodes for the circular and square domains, 10,903 nodes for the irregular 2D geometry, 18,494 nodes for the 3D problems, and these nodes are distributed uniformly.

Unless otherwise specified, the 2D test cases under complicated geometry have the same configuration of irregular geometry shown in Fig. 1(a) with the Neumann boundary condition specified at $x = 4$ boundary and the Dirichlet boundary condition at the rest of the boundary, where the small blank circles represent boundary knots. It is noted that this configuration involves corners, sharp notches, and interior elliptic cut-outs. These interior and exterior boundary shapes are deliberately designed to verify the robustness of the anisotropic BKM in solving arbitrary complicated geometric problems. For 3D cases, the configuration is displayed in Fig. 1(b), which is a cube centered at the origin with side-length 2, including a cutout sphere of radius 0.5. Both the Helmholtz-type and convection-diffusion problems are tested. Tables 1–8 show calculated results, where N is the total number of boundary knots with the BKM.

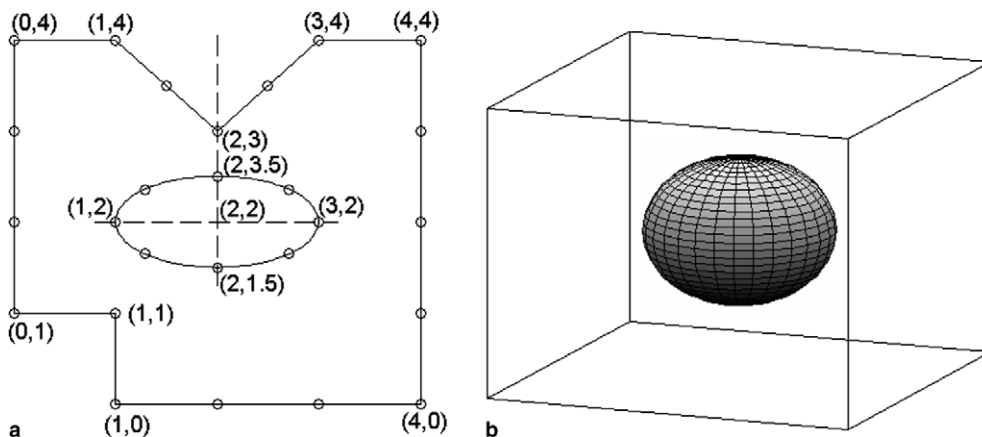


Fig. 1. Configurations of the 2D and 3D complicated geometries.

Table 1
Numerical results for 2D Helmholtz problem (26a)

N	rerr(u)	aerr(u)	merr(u)
16	4.1975e-3	1.7665e-3	1.0473e-2
20	8.8884e-6	3.7406e-6	3.2423e-5
24	1.9240e-6	8.0970e-7	1.0151e-5

Table 2
Numerical results for 2D Helmholtz problem (26b) with $\mu = 200$

N	rerr(u)	aerr(u)	merr(u)
480	9.4926e-3	9.4394e-3	8.8930e-2
500	1.6940e-5	1.6845e-5	1.4471e-4
520	9.0839e-7	9.0329e-7	3.2356e-6

Table 3
Numerical results for 2D Helmholtz problem (26b) with $\mu = 500$

N	rerr(u)	aerr(u)	merr(u)
1200	2.6618e-2	2.6511e-2	2.0579e-1
1230	4.4999e-3	4.4819e-3	1.1839e-1
1240	8.7123e-6	8.6774e-6	2.2138e-4
1250	8.0788e-6	8.0464e-6	6.3026e-5
1280	1.5261e-6	1.5200e-6	5.8993e-6

Table 4
Relative errors of 2D modified Helmholtz problem (28b)

N	rerr(u)	aerr(u)	merr(u)
11	3.9949e-4	9.0231e-4	3.4859e-3
16	8.6635e-7	1.9568e-6	8.4574e-6
20	5.3930e-8	1.2181e-7	1.1100e-6

Table 5
Relative errors of 2D convection-diffusion problem (30)

L	rerr(u)	aerr(u)	merr(u)
11	1.6517e-3	2.5522e-3	1.3992e-2
16	3.0256e-6	4.6751e-6	2.9927e-5
24	8.8356e-8	1.3653e-7	1.6875e-6

Table 6
Numerical results for 3D Helmholtz problem with analytical solution (35a)

N	rerr(u)	aerr(u)	merr(u)
18	4.0971e-2	2.7303e-2	1.1422e-1
31	1.7083e-3	1.1384e-3	7.5938e-3
61	2.0742e-5	1.3822e-5	8.1649e-5
105	9.1679e-8	6.1093e-8	6.3598e-7

3.1. 2D Helmholtz problems

The Helmholtz equation is frequently encountered in various fields of physical and engineering applications involving wave propagation and vibration phenomena, e.g., acoustics cavity, radiation, scattering, vibration [27,31–33], and electromagnetic field. We consider a 2D anisotropic Helmholtz equation

Table 7

Numerical results for 3D modified Helmholtz problem with analytical solution (35b)

N	rerr(u)	aerr(u)	merr(u)
16	9.3815e-3	3.5857e-2	1.9925e-1
29	7.0620e-4	2.6992e-3	3.4374e-2
61	3.9933e-6	1.5263e-5	1.2401e-4
105	2.0666e-7	7.8987e-7	6.2330e-6

Table 8

Numerical results for 3D convection-diffusion problem with analytical solution (35c)

N	rerr(u)	aerr(u)	merr(u)
18	8.2633e-3	3.1583e-2	1.8244e-1
30	1.6544e-4	6.3234e-4	5.9769e-3
61	1.3347e-6	5.1015e-6	4.9674e-5
105	5.9913e-8	2.2900e-7	2.5709e-6

$$\frac{\partial^2 u}{\partial x_1^2} + \frac{\partial^2 u}{\partial x_1 \partial x_2} + \frac{\partial^2 u}{\partial x_2^2} + \lambda^2 u = 0, \quad (x_1, x_2) \in \Omega. \quad (25)$$

Here the constant tensor k_{ij} is taken as $k_{ij} = 1/2 + 1/2\delta_{ij}$, where δ_{ij} is the Kronecker symbol. To illustrate the accuracy, we consider the problems with the following analytical solutions

$$u(x) = \sin\left(\frac{\sqrt{3}}{2}x_1\right) \sin\left(x_2 - \frac{x_1}{2}\right), \quad (26a)$$

$$u(x) = \sin\left(\frac{\sqrt{3}}{2}\mu x_1\right) + \cos\left(\mu\left(x_2 - \frac{x_1}{2}\right)\right). \quad (26b)$$

The wave number λ of the nonsingular general solution is $\sqrt{3}/2$ for the analytical solutions (26a), and $\sqrt{3}\mu/2$ for (26b). The Dirichlet and Neumann boundary conditions can be evaluated from the corresponding analytical solutions.

Fig. 2(a) displays the average relative error curves for a Dirichlet anisotropic problem with analytical solution (26a) on the circular and square domains. It is observed that the BKM solutions converge rapidly. The

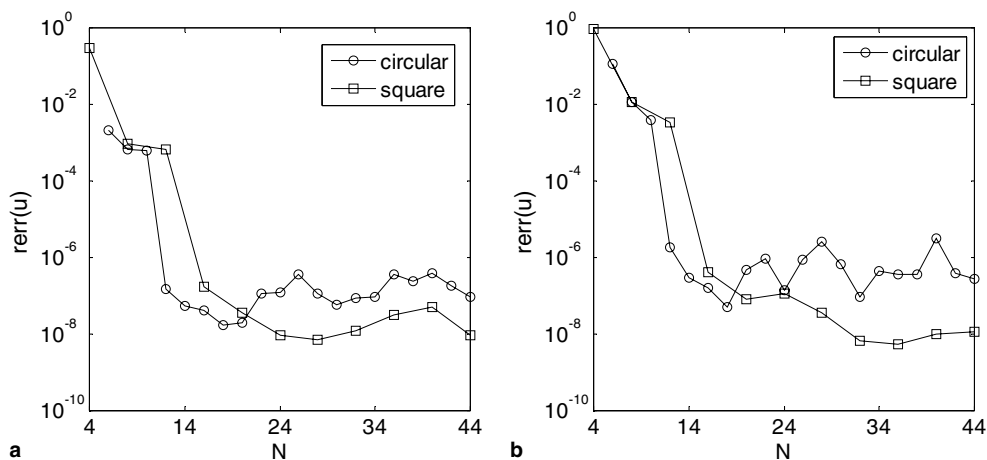


Fig. 2. Average relative error curves for the Helmholtz: (a) Dirichlet and (b) mixed boundary problems with the analytical solution given by (26a).

convergence rate for the Dirichlet Helmholtz problem is 12.9 for the circular and 9.8 for the square domain, respectively, prior to the minimum relative error value. Fig. 2(b) displays the average relative error for the anisotropic Helmholtz problem with the same analytical solution but subjected to a mix-type boundary condition, where the Neumann boundary condition is specified on the lower-half boundary of the circular domain and $x_2 = \pm 1$ boundary of the square domain. It is observed that the convergence rate of the mixed boundary value problem is slightly more rapid than the Dirichlet cases, being 15.1 for the circular and 10.2 for square domains.

To investigate the anisotropic Helmholtz problems with the moderate wave numbers, we consider the Dirichlet problem with analytical solution (26b). Fig. 3(a) and (b) shows the average relative error curves for $\mu = 20$ and $\mu = 50$ cases, respectively. It is observed from Fig. 3 that the higher wave number requires more boundary knots to achieve accurate results. It is interesting to note that for test case (26b) the higher the wave number, the larger the convergence rate. For example, the convergence rate for Helmholtz Dirichlet problem with $\mu = 20$ is 41.8 on the circular domain and 37.6 on the square domain, while it is 64.3 and 48.2 for either case, respectively when $\mu = 50$. The same observations persist for other distinct values of μ . For the sake of brevity, we do not present those results here.

To illustrate the wave property of the Helmholtz problem, Fig. 4 displays the solution profile and the absolute error surfaces in the square domain of the Helmholtz problem (26b) with $\mu = 20$ using 64, 80 and 120 boundary knots, respectively, where the error surfaces were yielded at 100×100 knots uniformly-spacing over the square. The solution accuracy is improved with the increase of boundary knots. Fig. 4(c) shows that errors around the corners are far pronounced in 80 knots BKM solutions.

We can see from Figs. 2 and 3 that the average relative error decreases steadily with the increasing boundary knots in the BKM, and then starts to oscillate when the solution reaches accuracy of certain degree. And the culprit for this phenomena may be ill-conditioning of the BKM interpolation matrix. The variation of the condition number (Cond) in terms of the knot number is shown in Fig. 5(a) for the Dirichlet Helmholtz problem. It is seen that the condition number increases steadily with the knot number, and then abruptly level off. If holding the knot number unchanged, the condition number decreases with the increasing wave number. Therefore, more knots in the BKM do not necessarily cause severe ill-conditioning for problems having a high wave number. The condition number for the mixed problem is displayed in Fig. 5(b) and behaves similarly as in the Dirichlet problem.

For a large number of knots, the BKM interpolation matrix equation tends to be severely ill-conditioned. However, the large condition number appears not necessarily to deteriorate the numerical results seriously. This paradox is also noted in various applications of the other RBF-based methods [12,14]. For large-scale problems, the domain decomposition method [3,20] could be used to reduce the condition number, and the fast multipole method [2] or hierarchical matrices are also promising in conjunction with the RBF-based

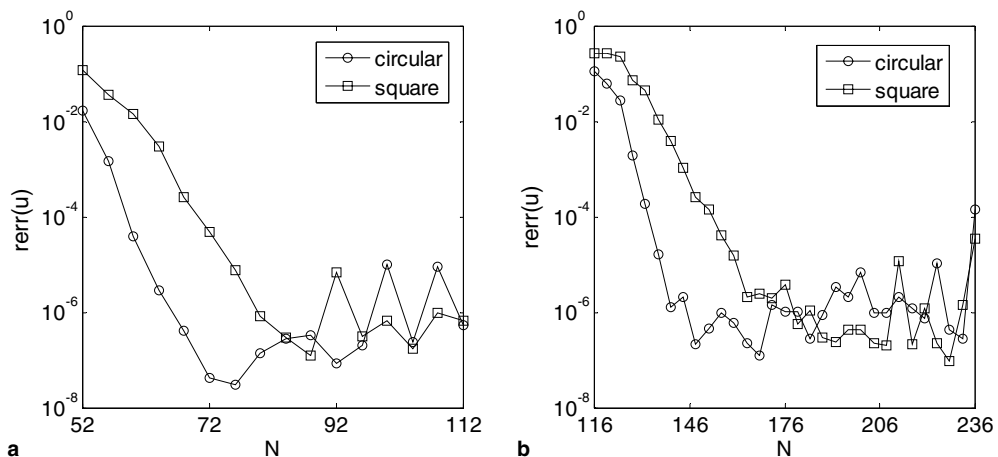


Fig. 3. Average relative error curves for Dirichlet Helmholtz problems (26b) with (a) $\mu = 20$ and (b) $\mu = 50$.

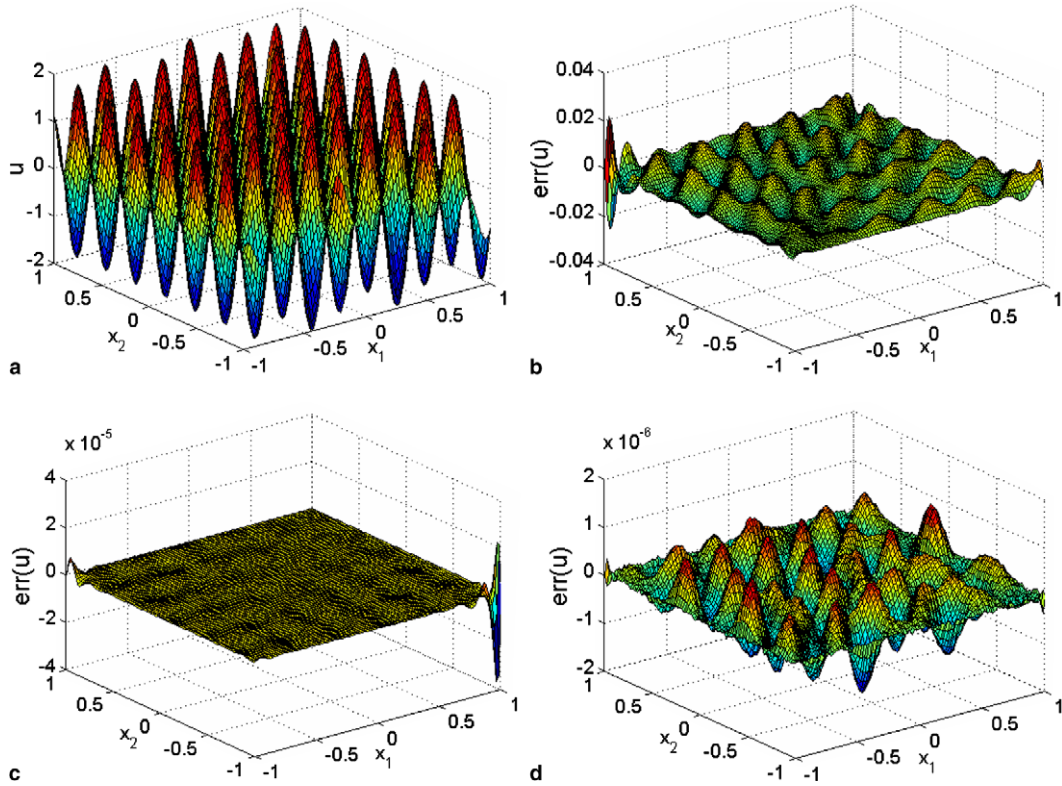


Fig. 4. Solution profile (a) and absolute error surfaces (b–d) of the anisotropic Dirichlet Helmholtz problem with wavenumber $\mu = 20$ having accurate solution (26b), where the BKM boundary knots are 64 for (b), 80 for (c) and 120 for (d), respectively.

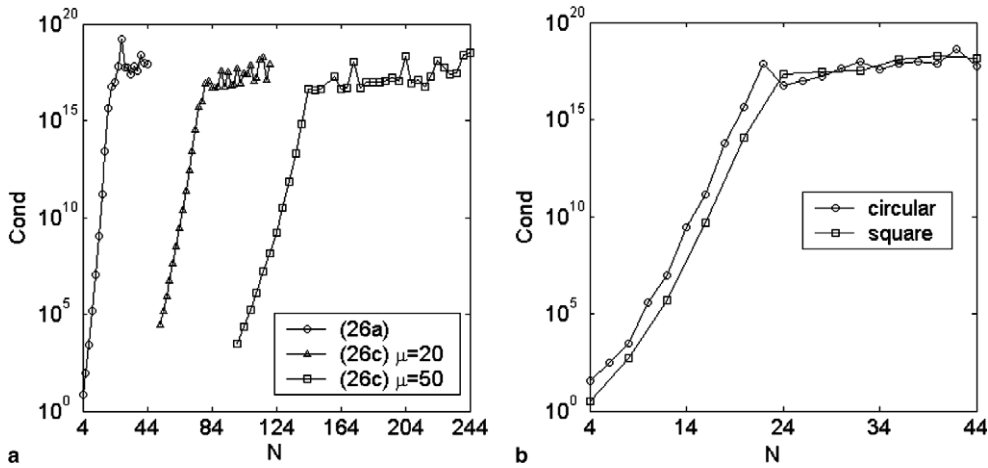


Fig. 5. The variation of the condition number against the knot number for: (a) Dirichlet problem on the circular domain and (b) mixed problem with analytical solution (26a).

methods. In case of noisy data of inverse problems, the ill-conditioning could pose a great numerical challenge, and various regularization methods [16] may be employed to stabilize the solution process.

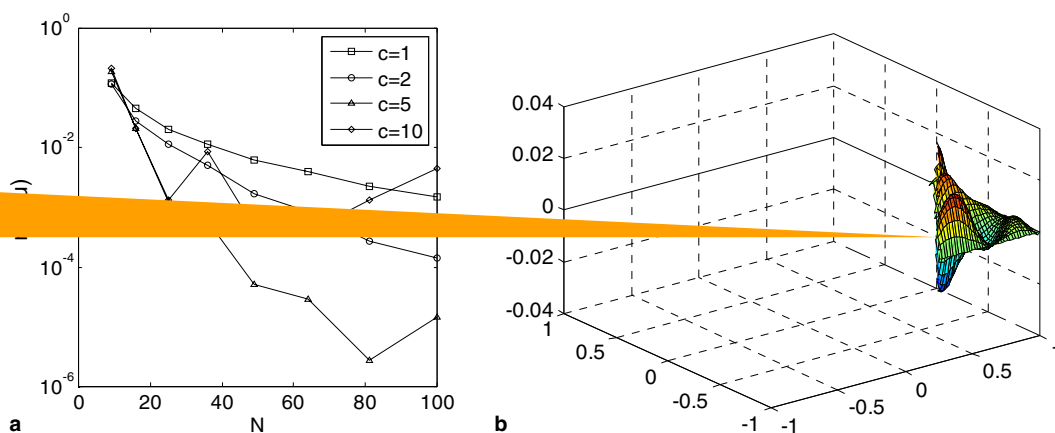
We also test the geodesic distance based BKM to the anisotropic Helmholtz problem under complicated geometry with the analytical solutions (26a). Table 1 displays the corresponding numerical results with

various numbers of knots. We can see that the present anisotropic BKM is stable, accurate and rapidly convergent. It is also observed that the BKM results with only 16 boundary knots are quite accurate for cases under physical domain having complicated-shaped exterior and interior boundaries. Many other numerical experiments were also performed in the preparation of this paper, and the same observations were found. It should be pointed out that the solutions on irregular domains are smooth. In the case that the solution has singularities, the numerical procedure could be far more complicated [21], and this is beyond the scope of the present study.

High wave number problems often pose a big challenge for accurate numerical solutions. For the finite element method to achieve an acceptable level of accuracy, more than 10 elements per wavelength should be used [25], which makes it very expensive for high wavenumber problems. To illustrate the potentiality of the proposed method for this kind problems, we present numerical results of the Helmholtz Dirichlet problem (26b) on a circular domain with $\mu = 200$ and $\mu = 500$ in Tables 2 and 3, respectively. From the numerical results presented, the fast convergence is observed, and the proposed method is promising.

Until now we consider only the numerical results by the proposed anisotropic method. To illustrate its merits and demerits versus the traditional isotropic distance based methods, Fig. 6(a) summarizes the numerical results of the Helmholtz Dirichlet problem (28a) on the square by the well-known isotropic multiquadric (MQ) RBF method, where c is the shape parameter in the MQ. Both methods produce comparable numerical results, provided that the shape parameter in the MQ is appropriately chosen. It's observed that the accuracy of the MQ RBF method depends significantly on the shape parameter, and an inappropriate choice of the shape parameter would deteriorate the accuracy significantly. The optimal shape parameter in the MQ is very difficult to determine a priori and remains a perplexing problem, while the geodesic BKM has no such a shape parameter problem.

As the wave number increases, the isotropic distance method has some difficulty in obtaining accurate results. Fig. 6(b) displays the error surface of the Helmholtz Dirichlet problem (26b) with $\mu = 20$ on the square domain by the MQ with 2116 uniformly-distributed collocation points. Here the shape parameter c is taken to be 0.5, which is determined via a trial error procedure. The accuracy of the numerical results is $rerr(u) = 9.5831e - 3$, $aerr(u) = 9.6136e - 3$ and $merr(u) = 2.9595e - 2$, whereas the present geodesic distance method using 64 nodes has $rerr(u) = 3.1024e - 3$, $aerr(u) = 3.1123e - 3$ and $merr(u) = 2.5698e - 2$. Therefore, the result by the isotropic MQ RBF method is slightly inferior to that by the present method using a relatively much smaller number of nodes. A close comparison of Fig. 6(b) with Fig. 4(b) also supports this argument. And our method incorporates the characteristic kernel solution of the problem of interest and reduces the dimensionality by one. From the above numerical results, we may conclude that the anisotropic BKM method is superior to the MQ RBF method based on isotropic basis functions for the homogeneous high wave number problems.



i. 6. (a) e aerae relatiae errr cure te uerical sluti r

3.2. 2D modified Helmholtz problems

The modified Helmholtz equation is used to model heat conduction [21,28] as well as in chemical reaction engineering, often referred to as the diffusion-reaction equation [1]. Consider a 2D anisotropic modified Helmholtz problem

$$5 \frac{\partial^2 u}{\partial x_1^2} + 4 \frac{\partial^2 u}{\partial x_1 \partial x_2} + \frac{\partial^2 u}{\partial x_2^2} - \lambda^2 u = 0, \quad (x_1, x_2) \in \Omega, \tag{27}$$

where $k_{11} = 5$, $k_{12} = 2$ and $k_{22} = 1$ consist in the constant tensor coefficient matrix k_{ij} . Consider the two test cases with the analytical solutions:

$$u(x) = \exp\left(-\frac{3x_1}{5} + 2x_2\right), \tag{28a}$$

$$u(x) = \exp\left(-\frac{3x_1}{10} + \frac{x_2}{2}\right). \tag{28b}$$

λ is taken to be 1 for the case (28a) and $1/\sqrt{10}$ for (28b), respectively. The Dirichlet and Neumann boundary conditions can be evaluated accordingly. The relative error against the knot numbers for test case (28a) are illustrated in Fig. 7(a). It is found that the anisotropic BKM converges stably and quickly, and the convergence rate is 15.8 and 12.6 for the circular and square domains, respectively. Furthermore, Fig. 7(b) shows that the BKM performs as well for the mixed-type boundary conditions, and the convergence rate is almost identical as in the Dirichlet case.

Fig. 8 displays the analytical solution profile of the Dirichlet problem on the square domain and the error surfaces of the BKM approximate solutions using 8, 12 and 20 boundary knots, where the error surfaces were yielded at 100×100 knots uniformly-spaced over the square. It is interesting to note that the error surfaces with 8 and 12 boundary knots are smooth, while that with 20 boundary knots is more roughly distributed.

Table 4 presents the numerical results for test case (28b) under the 2D complex-geometry. It is seen that 11 boundary knots make accurate solutions, and 16 knots suffice striking accuracy.

3.3. 2D convection-diffusion problems

The numerical solution of the convection-diffusion problem is often a difficult task largely because of troublesome convection term. Ref. [23] claims that the BEM outperforms the FEM and FDM in solving convection-diffusion problems because the convection terms have been inherently embedded in the fundamental

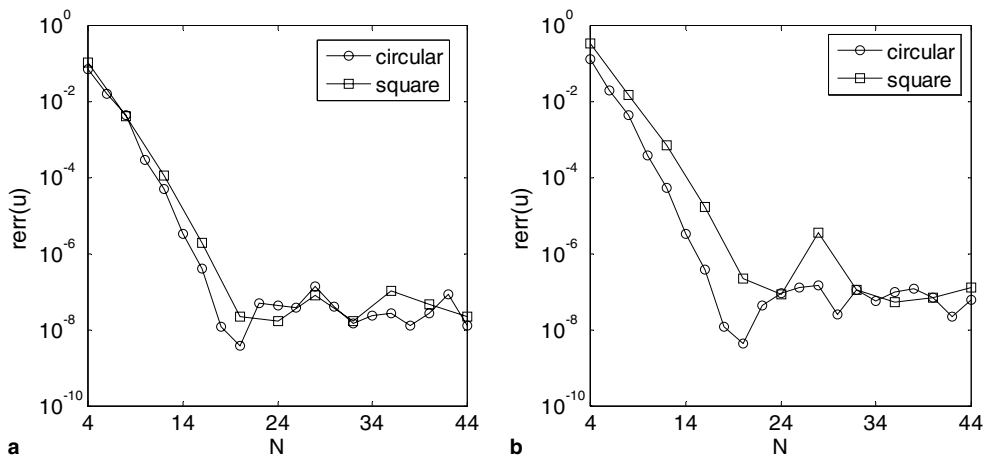


Fig. 7. Average relative error curves for the modified Helmholtz: (a) Dirichlet and (b) mixed problem (28a), respectively.

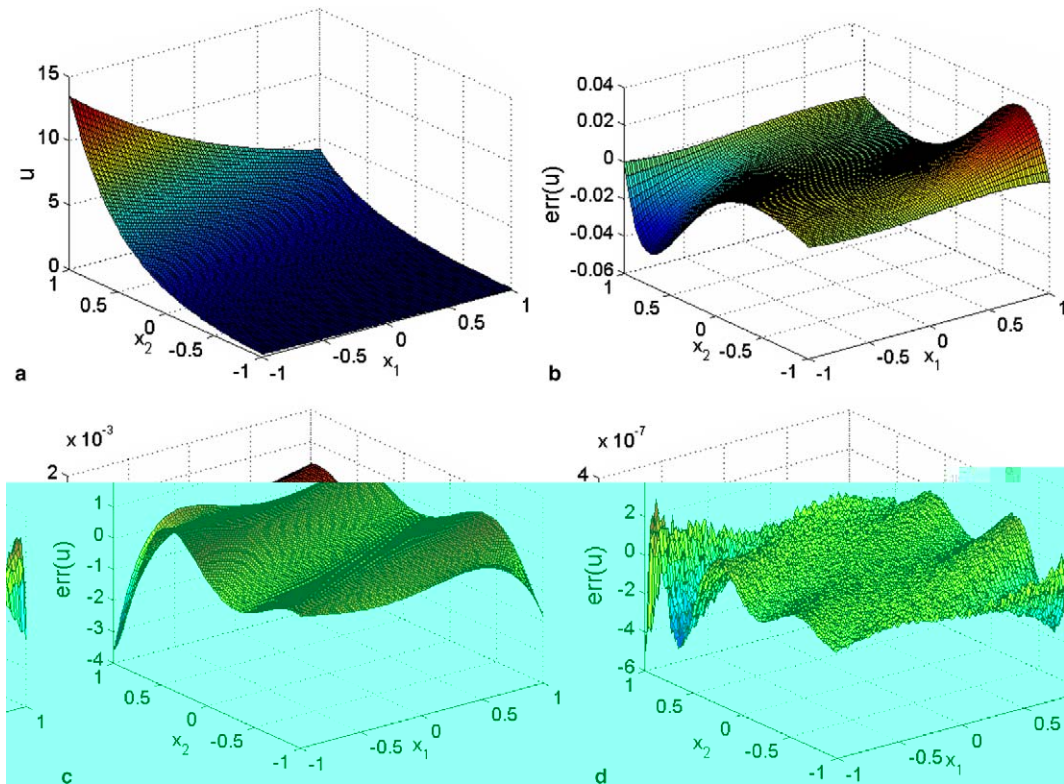


Fig. 8. (a) the solution profile of the modified Helmholtz problem (28a) and its error surfaces of the numerical solution using (b) 8, (c) 12 and (d) 20 boundary knots, respectively.

solution of the convection-diffusion operator, so is the case for the present anisotropic BKM [10]. For a clear illustration, we consider an anisotropic convection-diffusion problem

$$\frac{\partial^2 u}{\partial x_1^2} + \frac{\partial^2 u}{\partial x_1 \partial x_2} + \frac{\partial^2 u}{\partial x_2^2} + \mathbf{v} \cdot \nabla u = 0, \quad (x_1, x_2) \in \Omega, \tag{29}$$

where $k_{11} = k_{22} = 1$ and $k_{12} = 1/2$ in the constant tensor k_{ij} , and the velocity \mathbf{v} is given by

$$\mathbf{v} = \left(\frac{\sqrt{3}}{2} + \frac{3 + \sqrt{3}}{4} \right)^T.$$

The analytical solution of the test case is given by

$$u(x) = \exp\left(-\frac{\sqrt{3}}{2}x_1\right) + \exp\left(\frac{x_1}{2} - x_2\right). \tag{30}$$

Fig. 9(a) shows the relative error against the knot number for the above test case (30). As in the previous Helmholtz cases, it is observed that the anisotropic BKM converges stably and quickly, and the convergence rate is 13.2 for the circular domain and 10.1 for the square domain. Fig. 9(b) further shows that the anisotropic BKM performs equally well for the mixed-type boundary conditions, and the convergence rate is comparable with that of the Dirichlet case.

Table 5 presents the numerical results for test case (29) in the 2D complicated geometry. It is noted that 11 boundary knots could achieve good accuracy, and 24 knots suffice very high accuracy up to eight significant digits. The outstanding performances are because the BKM with the anisotropic convection-diffusion nonsingular solution could well capture the convective effects of the governing equation.

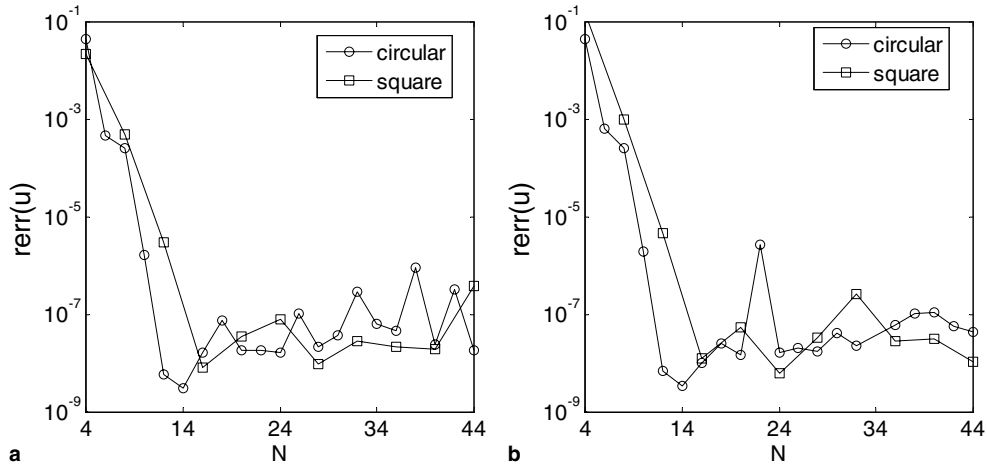


Fig. 9. Convergence curves of average relative error for the convection-diffusion (a) Dirichlet and (b) mixed problems with analytical solution (30), respectively.

3.4. Stability with respect to anisotropy

It is well known that the difficulty of anisotropic problems depends crucially on the determinant of the constant material tensor \mathbf{K} . Generally speaking, the smaller the determinant $\det(\mathbf{K})$, the more difficult is the anisotropic problem. To investigate the effect of anisotropy on the accuracy, we first consider an orthotropic case, where the cross-terms k_{ij} ($i \neq j$) vanish. In particular we consider the following equation:

$$\mu \frac{\partial^2 u}{\partial x_1^2} + \frac{\partial^2 u}{\partial x_2^2} + \lambda^2 u = 0, \quad (x_1, x_2) \in \Omega, \tag{31}$$

where $k_{11} = \mu, k_{12} = 1$, μ is a number dictating the anisotropy of the problem, and Ω is the circular domain. Therefore, the determinant $\det(\mathbf{K})$ is determined solely by the parameter μ . The Dirichlet condition is prescribed on $\partial\Omega$ such that its solution is given by

$$u(x) = \sin\left(\frac{x_1}{\sqrt{\mu}}\right) + \sin(x_2). \tag{32}$$

The wave number λ of the problem is kept 1 to investigate anisotropic influence of the value of μ on the numerical solution. We experimented the Helmholtz problem (32) with $\det(K)$ in the range $[1 \times 10^{-3}, 1 \times 10^6]$, and the results are summarized in Fig. 10(a).

From Fig. 10(a), it is observed that as the determinant $\det(K)$ increases from 1×10^{-3} to 1×10^6 , the accuracy of the numerical results increases steadily and then at some point start fluctuations for larger values of $\det(K)$. This is attributed to the ill-conditioning of the BKM interpolation matrix as discussed and analyzed before. It is stressed that the smaller the determinant, the greater the anisotropy. We see from Fig. 10(a) that more nodes are required in greater anisotropy to obtain accurate solutions. Smaller μ leads to smaller $\det(K)$ and greater anisotropy and also a higher frequency component in the first term of the solution (32). It is known that high-frequency problems require relatively more knots for accurate solutions. In this case, the wavenumber is in fact not determined by λ alone. And the effective wavenumber involves both λ and μ . And high anisotropy causes high wave number and increases the difficulty of numerical solutions.

Next we consider anisotropic problem with non-diagonal terms.

$$\frac{\partial^2 u}{\partial x_1^2} + 2\mu \frac{\partial^2 u}{\partial x_1 \partial x_2} + \frac{\partial^2 u}{\partial x_2^2} + \lambda^2 u = 0, \quad (x_1, x_2) \in \Omega, \tag{33}$$

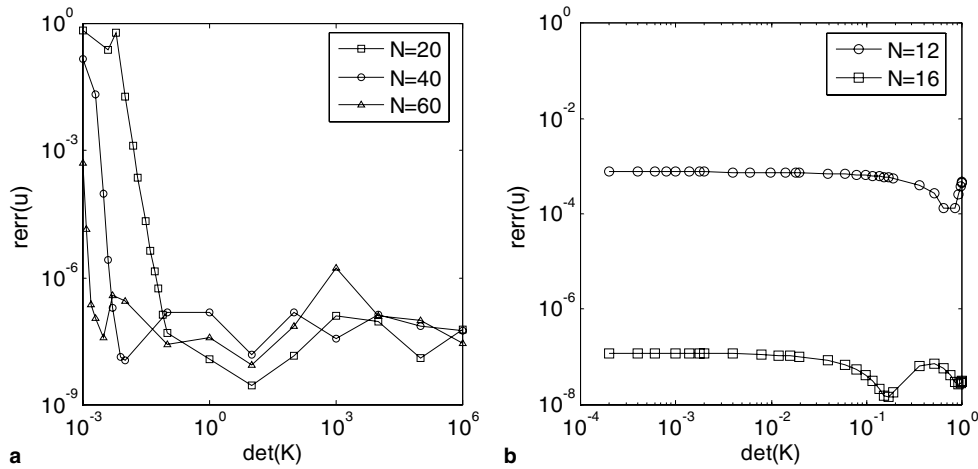


Fig. 10. The average relative error curves for the Helmholtz problem: (a) (32) and (b) (34) with respect to $\det(\mathbf{K})$.

where the constant tensor $k_{11} = k_{22} = 1$, and $k_{12} = \mu$. The parameter μ controls the degree of anisotropy of the problem, and we investigate the sensitivity of the numerical results with respect to anisotropy. The analytical solution is given by

$$u(x) = \sin\left(\sqrt{1 - \mu^2}x_1\right) \sin\left(x_2 - \mu x_1\right), \tag{34}$$

where the wave number λ is taken to be $\sqrt{2 - 2\mu^2}$.

The numerical results for the Helmholtz problem (34) on the circular domain are shown in Fig. 10(b). And we can see that the accuracy is almost independent of the determinant of the constant tensor when it is in the range $[2 \times 10^{-4}, 1]$.

3.5. 3D Helmholtz, modified Helmholtz and convection-diffusion problems

Three-dimensional problems are usually not easy to deal with by the traditional numerical techniques. This dimensional effect is often dubbed the curse of dimensionality and is one of the greatest barriers in higher-dimension computing. The following examples are intended to verify numerically the accuracy and efficiency of the present anisotropic BKM solution of 3D problems. The analytical solutions of our test cases are given by

$$u(x) = \sin\left(\frac{\sqrt{3}}{2}x_1\right) + \sin\left(x_2 - \frac{x_1}{2}\right) + \sin\left(\frac{\sqrt{2}}{4}(3x_3 - x_1 - x_2)\right), \tag{35a}$$

$$u(x) = \exp\left(\frac{\sqrt{3}}{2}x_1\right) + \exp\left(x_2 - \frac{x_1}{2}\right) + \exp\left(\frac{\sqrt{2}}{4}(3x_3 - x_1 - x_2)\right), \tag{35b}$$

$$u(x) = \exp\left(-\frac{\sqrt{3}}{2}x_1\right) + \exp\left(\frac{x_1}{2} - x_2\right) + \exp\left(\frac{\sqrt{2}}{4}(x_1 + x_2 - 3x_3)\right), \tag{35c}$$

for the Helmholtz, modified Helmholtz and convection-diffusion equations, respectively. The constant tensor k_{ij} is taken as $k_{ij} = 1/2 + 1/2\delta_{ij}$. λ in the nonsingular general solution is taken $\sqrt{3}/2$, $\sqrt{3}/2$ and zero for the Helmholtz, modified Helmholtz and convection-diffusion equations, respectively. The velocity vector \mathbf{v} for the convection-diffusion problem is

$$\mathbf{v} = \left(\frac{\sqrt{3}}{2}, \frac{3 + \sqrt{3}}{4}, \frac{\sqrt{2}}{2} + \frac{1 + \sqrt{3}}{4}\right)^T.$$

The numerical results for test case (35a) are displayed in Tables 6. The anisotropic BKM is found to work as well for this 3D problem as in the previous 2D cases. With a few dozen points, the geodesic distance based BKM produces remarkably accurate results. The similar observations also appear in test cases (35b) and (35c), shown in Tables 7 and 8, respectively. It should be noted that 29 knots yield the accuracy of seven significant digits for the 3D convection-diffusion problems. This indicates that the anisotropic BKM may be a competitive alternative to tackle high-dimensional anisotropic problems effectively.

It is stressed that compared with the 2D problems, no extra coding effort is required for the 3D cases, except of a single line of the different definition of the distance variable. The BKM demands neither domain nor boundary grid generations, a considerable saving compared with mesh-based methods, where high quality meshing of 3D complicated geometry could be computationally very expensive.

4. Concluding remarks

The extension of the RBF-based numerical techniques to the anisotropic problems is practically significant in many real-world applications, where anisotropic media are pronouncedly present. The BKM can be considered a particular type of RBF-based methods where the general solution RBF is used to evaluate the homogeneous solution and the DRM and RBF calculates the particular solution. In this study, the geodesic distance replaces the standard isotropic Euclidean distance in the BKM to solve the anisotropic Helmholtz, diffusion, and convection-diffusion problems under 2D and 3D complicated geometries. The numerical results confirm that this strategy works successfully for the tested cases. This will encourage the use of the other problem-dependent definition of distance [8] in the RBF methods for engineering problems having strong features such as a preferred direction. The geodesic distance-based Kansa's method, a domain type RBF technique, is now under investigation for anisotropic problems.

Acknowledgements

We thank the anonymous reviewers of this paper for their very helpful comments and suggestions to significantly improve the academic quality of this paper. The work described in this paper was supported by a research project funded by the National Natural Science Foundation of China (Project No. 10442001) and a grant from the CAEP, China (Project No. 20050651). The second author gratefully acknowledges the support of K. C. Wong Education Foundation, Hong Kong.

References

- [1] K. Balakrishnan, P.A. Ramachandran, The method of fundamental solutions for linear diffusion-reaction equations, *Math. Comput. Model.* 31 (2000) 221–237.
- [2] R.K. Beatson, J.B. Cherrie, C.T. Mouat, Fast fitting of radial basis functions: methods based on preconditioned GMRES iteration, *Adv. Comput. Math.* 11 (1999) 253–270.
- [3] H. Brown, L. Ling, E.J. Kansa, On approximate cardinal preconditioning methods for solving PDEs with radial basis functions, *Eng. Anal. Bound. Elem.* 29 (2005) 343–353.
- [4] C.S. Chen, M.A. Golberg, R.S. Schaback, Recent developments of the dual reciprocity method using compactly supported radial basis functions, in: Y.F. Rashed, C.A. Brebbia (Eds.), *Transformation of Domain Effects to the Boundary*, WIT Press, Southampton, Boston, 2003, pp. 183–225.
- [5] J.T. Chen, M.H. Chang, K.H. Chen, S.R. Lin, The boundary collocation method with meshless concept for acoustic eigenanalysis of two-dimensional cavities using radial basis function, *J. Sound Vib.* 257 (2002) 667–711.
- [6] J.T. Chen, M.H. Chang, K.H. Chen, I.L. Chen, Boundary collocation method for acoustic eigenanalysis of three-dimensional cavities using radial basis function, *Comput. Mech.* 29 (2002) 392–408.
- [7] J.T. Chen, M.H. Chang, I.L. Chung, Y.C. Cheng, Comment on “Eigenmode analysis of arbitrarily shaped two-dimensional cavities by the method of point matching”, *J. Acoust. Soc. Am.* 111 (2002) 33–36.
- [8] W. Chen, Definitions of distance function in radial basis function approach, CoRR online preprint, cs.CE/0207018, 2002.
- [9] W. Chen, Distance function wavelets – Part III: “Exotic transforms and series, Research report of Simula Research Laboratory, CoRR preprint, available form: <<http://arxiv.org/abs/cs.CE/0206016>> June, 2002.
- [10] W. Chen, Y.C. Hon, Numerical convergence of boundary knot method in the analysis of Helmholtz, modified Helmholtz, and convection-diffusion problems, *Comput. Meth. Appl. Mech. Eng.* 192 (2003) 1859–1875.
- [11] W. Chen, M. Tanaka, A meshless, integration-free, and boundary-only RBF technique, *Comput. Math. Appl.* 43 (2002) 379–391.

- [12] H. Ding, C. Shu, K.S. Yeo, Local radial basis function-based differential quadrature method and its application to solve two-dimensional incompressible Navier-Stokes equations, *Comput. Methods Appl. Mech. Eng.* 192 (2003) 941–954.
- [13] R. Franke, Scattered data interpolation: tests of some methods, *Math. Comput.* 38 (1982) 181–200.
- [14] M.A. Golberg, C.S. Chen, The method of fundamental solution for potential, Helmholtz and diffusion problems, in: Golberg (Ed.), *Boundary Integral Methods: Numerical and Mathematical Aspects*, Computational Mechanics Publications, Southampton, 1998, pp. 103–176.
- [15] M.A. Golberg, C.S. Chen, H. Bowman, Some recent results and proposals for the use of radial basis functions in the BEM, *Eng. Anal. Bound. Elem.* 23 (1999) 285–296.
- [16] P.C. Hansen, *Rank-Deficient and Discrete Ill-posed Problems: Numerical Aspects of LSIAM*, SIAM, Philadelphia, 1998.
- [17] Y.C. Hon, X.Z. Mao, A radial basis function method for solving options pricing model, *Financ. Eng.* 81 (1999) 31–49.
- [18] E.J. Kansa, Multiquadrics: A scattered data approximation scheme with applications to computational fluid dynamics, *Comput. Math. Appl.* 19 (1990) 147–161.
- [19] J. Li, Mathematical justification for RBF-MFS, *Eng. Anal. Bound.* 25 (2001) 897–901.
- [20] L. Ling, E.J. Kansa, Preconditioning for radial basis functions with domain decomposition methods, *Math. Comput. Model.* 40 (2004) 1413–1427.
- [21] L. Marin, D. Lesnic, V. Mantic, Treatment of singularities in Helmholtz-type equations using the boundary element method, *J. Sound Vib.* 278 (2004) 39–62.
- [22] D. Nardini, C.A. Brebbia, A new approach to free vibration analysis using boundary elements, *Appl. Math. Model.* 7 (1983) 157–162.
- [23] P.W. Partridge, C.A. Brebbia, L.W. Wrobel, *The Dual Reciprocity Boundary Element Method*, Computational Mechanics Publication, Southampton, 1992.
- [24] Y.C. Shiah, C.L. Tan, BEM treatment of two-dimensional anisotropic field problems by direct domain mapping, *Eng. Anal. Bound. Elem.* 20 (1997) 347–351.
- [25] C. Shu, H. Xue, Solution of Helmholtz equation by differential quadrature method, *Comput. Methods Appl. Mech. Eng.* 175 (1999) 203–212.
- [26] J. Sladek, V. Sladek, S.N. Atluri, Meshless local Petrov–Galerkin method for heat conduction problem in an anisotropic medium, *CMES-Comput. Model. Eng. Sci.* 6 (2004) 309–318.
- [27] J. Wang, J.B. Lin, A two-dimensional theory for surface acoustic wave propagation in finite piezoelectric solids, *J. Intell. Mater. Syst. Struct.* 16 (2005) 623–629.
- [28] A.S. Wood, G.E. Topholme, M.I.H. Bhatti, P.J. Heggs, Steady-state heat transfer through extended plane surfaces, *Int. Comm. Heat Mass Transfer* 22 (1995) 99–109.
- [29] J.M. Zhang, M. Tanaka, M. Endo, The hybrid boundary node method accelerated by fast multipole method for 3D potential problems, *Int. J. Numer. Method. Eng.* 63 (2005) 660–680.
- [30] J.M. Zhang, M. Tanaka, T. Matsumoto, A simplified approach for heat conduction analysis of CNT-based nano-composites, *Comput. Method. Appl. Mech. Eng.* 193 (2004) 5597–5609.
- [31] X. Zhang, K.Z. Song, M.W. Lu, Meshless methods based on collocation with radial basis functions, *Comput. Mech.* 26 (2000) 333–343.
- [32] X. Zhang, X.H. Liu, K.Z. Song, M.W. Lu, Least-square collocation meshless method, *Int. J. Numer. Method. Eng.* 51 (2001) 1089–1100.
- [33] H.Z. Zhong, Q. Guo, Vibration analysis of rectangular plates with free corners using spline-based differential quadrature, *Shock Vib.* 11 (2004) 119–128.